ACS SyntheticBiology

Research Article

pubs.acs.org/synthbio

Solution Structure of a Bacterial Microcompartment Targeting Peptide and Its Application in the Construction of an Ethanol Bioreactor

Andrew D. Lawrence,[†,#] Stefanie Frank,[†,#] Sarah Newnham,[†] Matthew J. Lee,[†] Ian R. Brown,[†] Wei-Feng Xue,[†] Michelle L. Rowe,[†] Daniel P. Mulvihill,[†] Michael B. Prentice,[‡,§] Mark J. Howard,[†] and Martin J. Warren*[,†]

[†]School of Biosciences, University of Kent, Giles Lane, Canterbury, Kent CT2 7NJ, U.K.

[‡]Department of Microbiology and [§]Department of Pathology, University College Cork, Cork, Ireland

Supporting Information

ABSTRACT: Targeting of proteins to bacterial microcompartments (BMCs) is mediated by an 18-amino-acid peptide sequence. Herein, we report the solution structure of the N-terminal targeting peptide (P18) of PduP, the aldehyde dehydrogenase associated with the 1,2-propanediol utilization metabolosome from *Citrobacter freundii*. The solution structure reveals the peptide to have a well-defined helical conformation along its whole length. Saturation transfer difference and transferred NOE NMR has highlighted the observed interaction surface on the peptide with its main interacting shell protein, PduK. By tagging both a pyruvate decarboxylase and an alcohol dehydrogenase with targeting peptides, it has been possible to direct these enzymes to empty BMCs *in vivo* and to generate an ethanol bioreactor. Not only are the purified, redesigned BMCs able to transform pyruvate into ethanol efficiently, but the strains containing the modified BMCs produce elevated levels of alcohol.

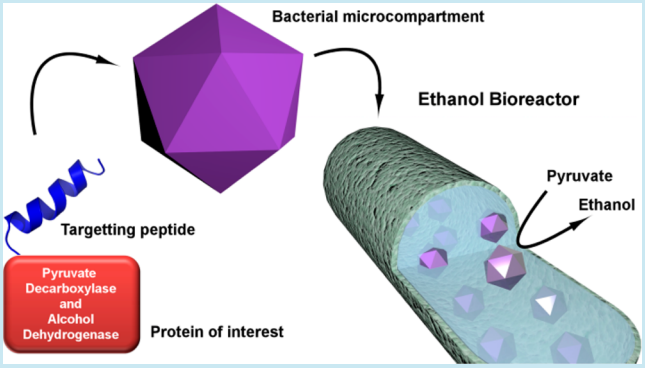

KEYWORDS: *metabolic engineering, compartmentalization, propanediol utilization, synthetic biology*

Bacterial microcompartments (BMCs) are discrete metabolic units found in a range of bacteria that are dedicated to a specific metabolic pathway.[1] They consist of a semipermeable proteinaceous outer layer that encases enzymes associated with a particular process. The best characterized of the BMCs is the carboxysome, which is found in cyanobacteria and some chemoautotrophs.[2−7] Here, the enzymes carbonic anhydrase and RuBisCo are retained within the confines of the macromolecular complex to provide an environment for enhanced carbon dioxide fixation. Other examples of the BMCs include the metabolosomes associated with both 1,2-propanediol and ethanolamine utilization.[8−13] Of these the former has been the subject of greater investigation and characterization.

The propanediol utilization (*pdu*) operon is composed of 23 genes[11,14,15] and encodes largely for proteins that form a supramolecular complex in the form of a metabolosome[13] with a diameter of between 100 and 150 nm. Six of the genes (*pduABJKUT*) encode for shell proteins that form hexameric tiles, which are envisaged to align together to form the facets and edges of the outer casing of the structure.[16−19] The vertices of the BMCs are thought to be formed from the pentameric PduN.[7,20] The shell proteins snare the enzymes for 1,2-propanediol metabolism, including the diol dehydratase (PduCDE), and the alcohol and aldehyde dehydrogenases (PduP and Q).[8,11] The metabolosome also houses enzymes for the repair and reactivation of the diol dehydratase (PduG, H) and its coenzyme (PduO, S), adenosylcobalamin.[8,11] The shell of the metabolosome has to allow the passage of its substrates, cofactors, and coenzymes into the bacterial microcompartment as well as the exit of the metabolic products.[18,21,22] This is likely mediated through the central pores that are formed within the tiles of the shell structure.[16,23] Other proteins are thought to interact with the shell proteins on the external surface of the structure, including PduV, which may help to localize the metabolosome within the cell.[24] A summary of the proposed Pdu BMC is given in Figure 1.

We have shown that it is possible to generate recombinant microcompartments in *Escherichia coli*, through the transposition of the whole *pdu* operon from *Citrobacter freundii* to generate fully functional metabolosomes.[11] More recently it has also been reported that recombinant carboxysomes can be

Received: August 15, 2013
Published: January 30, 2014

dx.doi.org/10.1021/sb4001118 | *ACS Synth. Biol.* 2014, 3, 454−465

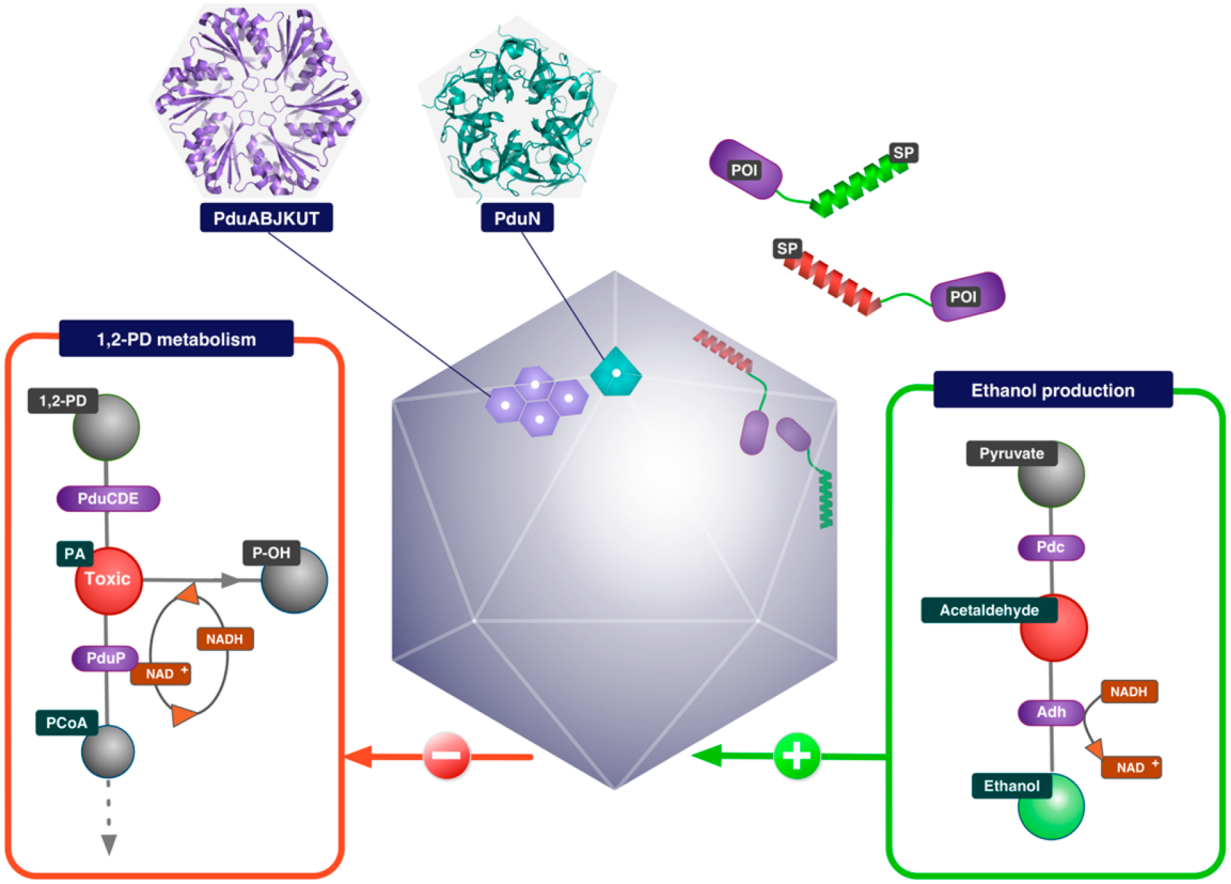

Figure 1. Steps required for the conversion of the 1,2-propanediol utilization (Pdu) microcompartment into an ethanol bioreactor. The Pdu microcompartment shell is built from hexameric tiles composed of PduA, B, J, K, U, and T (purple) that form the facets of the structure, whereas pentameric tiles (PduN, cyan) form the vertices. 1,2-Propanediol enters the shell through pores in the shell proteins and is metabolized to propionyl-CoA (red box), which leaves the compartment and is further converted to propionate. Enzymes that are encapsulated within the metabolosome contain short signaling peptides. Changing the specificity of the Pdu microcompartment is achieved by stripping out the Pdu pathway and replacing it with the required pathway, *e.g.*, ethanol production (green box). Fusion of signaling peptides to the new pathway enzymes facilitates association of the heterologous proteins. Abbreviations used in figure: 1,2-PD = 1,2-propanediol, PA = propionaldehyde, P-OH = 1-propanol, PCoA = propionyl-CoA, POI = protein of interest, SP = signaling peptide, Adh = Alcohol dehydrogenase, Pdc = pyruvate decarboxyase.

produced in *E. coli*.[25] Through the coordinated production of just the Pdu shell proteins empty microcompartments can be constructed within the cell.[24] A minimal set of shell proteins, PduABJKN, appears to be required for the assembly of empty metabolosomes, although slightly larger units are formed if PduU is included with the other shell proteins. Proteins can be targeted to these empty microcompartments by tagging them to other proteins that are found associated with the BMCs such as PduC, PduD, and PduV.[24] The potential therefore exists to generate new bioreactors within the molecular scaffold of a bacterial microcompartment[1] (Figure 1).

Key to understanding how BMCs form is the localization of the metabolic enzymes to the inside of the structure. One possibility, similar to the model suggested for carboxysome construction,[4,26,27] is that a lattice of shell and cargo protein forms simultaneously during assembly. It is known that encapsulation of some of the enzymes is dependent upon the presence of a peptide targeting sequence.[28,29] It could be that the targeting sequences encourage oligomerization around which the BMC forms. The targeting sequence appears to be located on either the N- or C-terminal region of the internalized protein,[30] although the structural features associated with these interactions have yet to be determined. For proteins such as PduP and PduD this targeting sequence can be very short, comprising around 18 amino acids.[28,29] Sequence analysis predicts that these targeting sequences are likely to be helical in nature. Herein, we provide the solution structure of the N-terminal 18 amino acids of PduP from *C. freundii* and show how this peptide sequence, together with a similar peptide from PduD, can be used to generate a simple ethanol bioreactor within a Pdu microcompartment shell by targeting the *Zymomonas mobilis* enzymes pyruvate decarboxylase (Pdc) and alcohol dehydrogenase (Adh) to the complex.

RESULTS AND DISCUSSION

PduP Interacts with PduK. Previous research has shown that the N-terminal region of the *Salmonella enterica* PduP is effective in targeting protein to the BMC.[24,29] In order to determine which of the shell proteins interact with PduP, we conducted a series of pull-down assays in which the *C. freundii* PduP was co-produced in *E. coli* along with individual shell proteins harboring an N-terminal poly histidine tag. Co-purification of PduP alongside a His-tagged shell protein following immobilized metal affinity chromatography (IMAC) is indicative of a protein−protein interaction and the formation of a tight complex. Using this method, we observed that PduP and PduK purified together (Supplementary Figure 1). An interaction between PduP and the shell proteins PduA and

dx.doi.org/10.1021/sb4001118 | *ACS Synth. Biol.* 2014, 3, 454−465

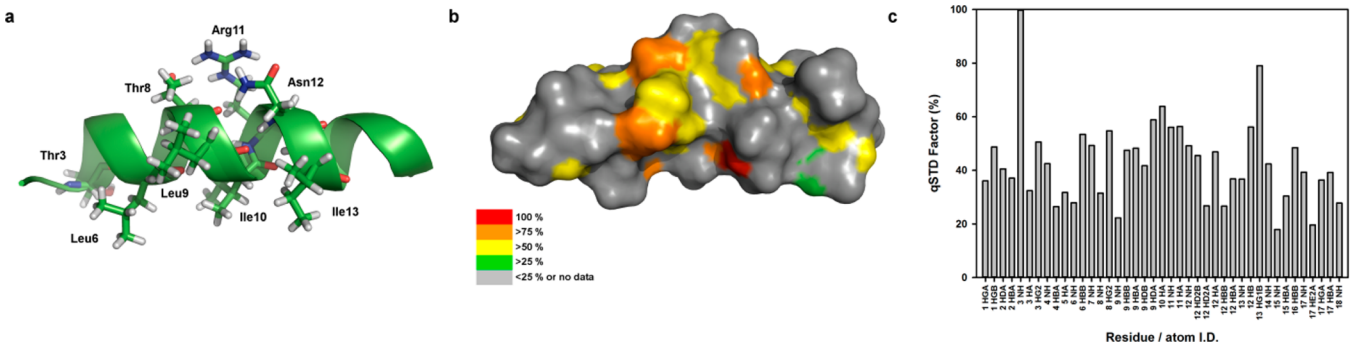

Figure 2. Solution structure of the P18 peptide and illustration of its interaction surface. (a) Solution structure of the P18 peptide highlighting the residues with the highest qSTD factors for the interaction between the peptide and the shell protein PduK. (b) Structure of the P18 peptide showing the solvent-accessible surface colored as a percentage of the maximum STD transfer to highlight significant interactions across the face of the helix. (c) Tabular representation of the relative qSTD amplification factors for the P18/PduK interaction.

PduJ from *Salmonella enterica* has been previously reported.[31] Although these results were not directly reproducible within our system, we did observe that co-production of PduP with PduA resulted in a shift of the proteins from the soluble to the insoluble fraction. PduK is known to be an abundant constituent of the shell, and its interaction with the P18 peptide (the first 18 amino acids of the N-terminus of PduP) was further investigated. To determine the binding constant for the interaction between the P18 peptide and PduK, we monitored the intrinsic tryptophan fluorescence of PduK, which contains only one tryptophan residue. Titration of P18 into a solution of PduK resulted in quenching of the fluorescence signal from the tryptophan. An equation describing a hyperbolic decay was fitted to the data, yielding a K_d of 331 ± 64 nM (Supplementary Figure 2). This titration was further evidence of a strong interaction between P18 and PduK. Moreover, the K_d is in a range that is acquiescent for STD NMR.[32]

PduK (156 amino acids) is larger than shell proteins such as PduA, PduJ, and PduU as it contains a C-terminal extension that has been speculated to house a Fe-S center.[16] To investigate if P18 binds to the BMC domain within PduK or whether it interacts with the C-terminal region of the protein, a truncation of the protein was made that consisted only of the first 96 amino acids. This truncated variant of PduK was also found to interact with P18 and with a K_d similar that of to the full-length protein.

Solution Structure of the P18 Peptide. The N-terminal region of PduP, which is responsible for the incorporation of the PduP enzyme into the lumen of the microcompartment, is suggested to be helical by both secondary structure prediction and CD spectroscopy.[31] Since there is no crystal structure available for this region of PduP or its homologues, we decided to solve the solution structure of the synthetic P18 peptide using NMR spectroscopy.

The structure of the P18 peptide (NH_3-MNTSELETLIRNL-ISEQL) was determined using primarily NOE through-space contacts by ^{1}H NMR in both the presence and absence of 30% (v/v) trifluoroethanol (TFE). Chemical shift assignments and through-space structural information were obtained from two-dimensional TOCSY and NOESY NMR experiments (Supplementary Table 1 and Supplementary Figure 3). The observed NOE contacts support the presence of an α-helical conformation of the peptide with NOEs observed between Hα and H_N (i−i+3) as well as Hα and Hβ (i−i+3) in both the presence and absence of TFE (Supplementary Figures 2a and 4 and Supplementary Table 2). The structural statistics table (Supplementary Table 2) demonstrate both structures provided expected Ramachandran plot statistics, similar Lennard-Jones energies, and small (<0.39 Å) backbone root mean squared deviation (rmsd) values for 20 calculated structures. These data are commensurate with recent studies of helical peptides[33,34] and suggest the data is robust. Furthermore, the extremely low level of NOE and dihedral violations suggest the data supplied for each structure was optimal.

Calculated structures demonstrate the formation of a continuous α-helix between residues 3 and 16 (Supplementary Figure 4). Important NOE contacts that define the structure of each peptide are summarized in Supplementary Figures 6 and 7. This is despite assignable Hα-H_N and Hα-Hβ i−i+3 NOEs not being continuous across the entire range of the helix due to spectral overlap. The presence of additional side chain i−i+3 NOEs and weak Hα-H_N i−i+4 NOEs confirm the continuity of the helix. It is important to note that the helical nature of the peptide in the absence of TFE suggests the P18 peptide may form a coiled-coil dimer in solution. This is supported by the small (<200 ms) NOE mixing times used to obtain structural information together with the fact that the sequence is amphipathic in nature. The addition of TFE, which is typically used as a stabilizer to aid secondary structure formation in short peptides, reduces the length of the helix (residues 5−15) and increased flexibility of the termini when compared to P18 in the absence of TFE (Supplementary Figure 4). The dualities of TFE acting as both a stabilizer of secondary structure and also as a denaturant has been studied and documented.[35] In this case, TFE has acted to destabilize the native structure of the P18 peptide, possibly through disruption of the coiled-coil conformation mentioned above. This would also explain the increased secondary structure definition in the P18 peptide in absence of TFE (Supplementary Figures 6 and 7) where increased helix length and stability is provided by a coiled-coil conformation. Regardless, the data suggest that the helical secondary structure element must be central to the process of recognition between the shell proteins and the PduP targeting sequence.

Saturation Transfer Difference (STD) NMR. The interaction between the P18 peptide and the shell protein PduK was investigated by 1D saturation transfer difference (STD) NMR (Supplementary Figure 5). This technique permits the detection of transient binding of a small molecule to a larger protein or receptor and can be used to determine molecular regions of the ligand that have primary contact and

dx.doi.org/10.1021/sb4001118 | *ACS Synth. Biol.* 2014, 3, 454−465

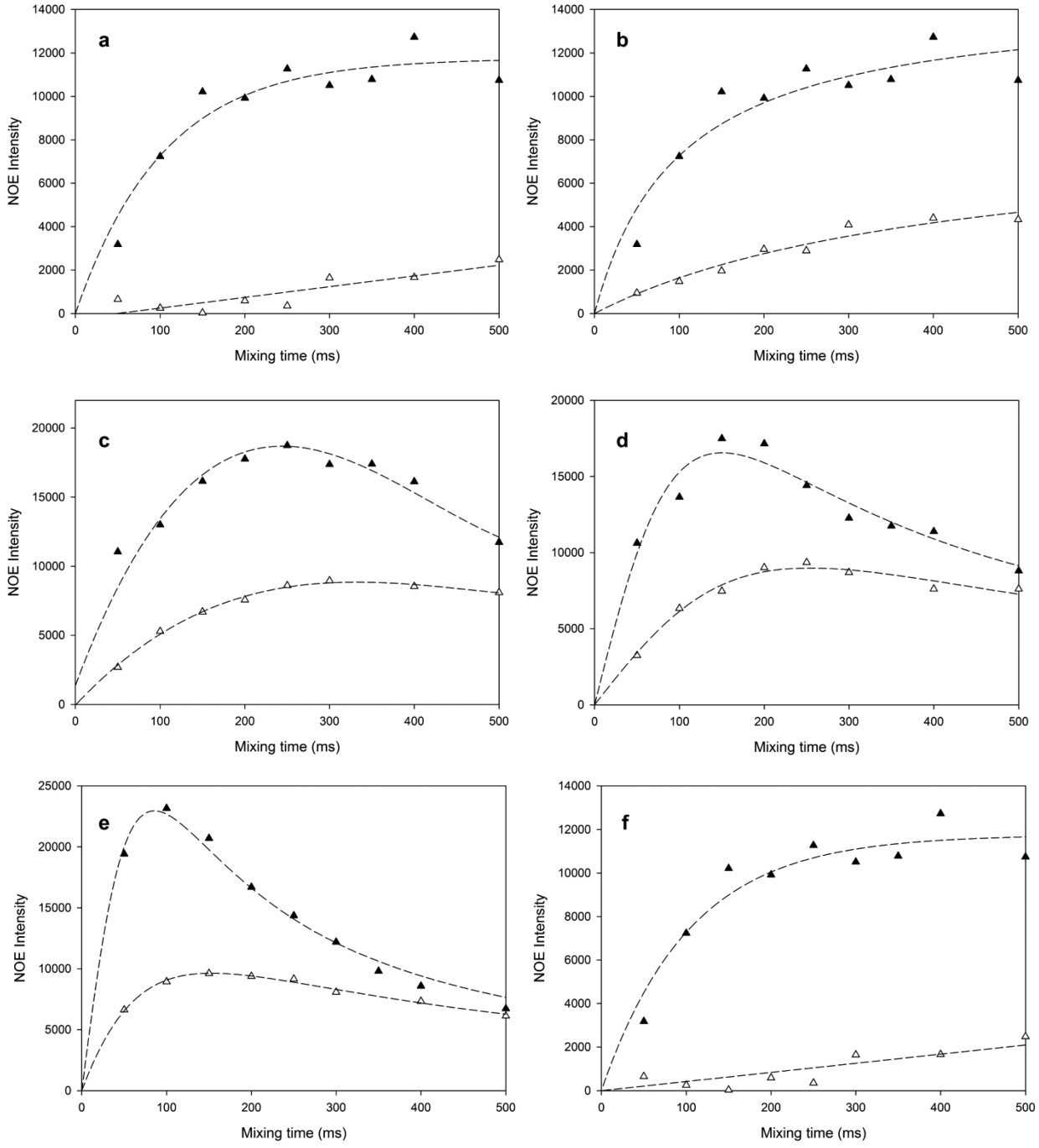

Figure 3. Transferred NOE build-up rates for the P18 peptide in the presence of PduK. Various NOE build-up curves for the P18 peptide in the absence (△) and presence (▲) of PduK. (a) 4SerH to 3ThrH, (b) 6LeuH to 3ThrHg2*,(c) 6LeuH to 3ThrHa, (d) 8ThrH to 5GluHa, (e) 12AsnH to 13IleH, (f) 16GluHga to 13IleHg2*. The peptide to protein ratio was 15:1.

are most likely responsible for recognition and binding to the protein of interest. Due to spectral crowding it was not possible to obtain unambiguous STD values for all protons in the P18 peptide, and only resonances that were not overlapping were used in the subsequent calculations and analysis. As a result of spectral overlap, it was important to corroborate the STD NMR data with transferred NOE data shown below. ^{1}H T_1 and STD NMR contributions were obtained through correlation of signal intensity to specific nuclei from the peptide. STD factors were modified according to the T_1 relaxation rate to provide a quantitative STD (qSTD) contribution (Supplementary Table 3). These values were displayed as percentage transfer compared to the maximum value (Figure 2c), and these data were mapped onto the calculated helical structure of the peptide (in the absence of TFE) to illustrate the observed interaction surface (Figure 2a and b). The residues with maximal STD factors highlight the center of one face of the helix and support an interaction with PduK despite the potential presence of a coiled-coil conformation for the free peptide. A comparison of N- or C-terminal BMC-targeting sequences has highlighted a number of conserved hydrophobic residues.[30] There would appear to be an apparent motif consisting of two hydrophobic residues followed by two polar residues followed by a further two hydrophobic residues. This

dx.doi.org/10.1021/sb4001118 | ACS Synth. Biol. 2014, 3, 454−465

represents the LIRNIL region in the center of the P18 sequence that corresponds with those residues reported with the highest STD values. These observations suggest the LIRNIL region is a putative binding patch on the P18 peptide.

Transferred NOE. The conformation of the P18 peptide while bound to PduK was investigated by NMR using transferred NOEs (trNOE). The trNOE allows structural information to be gathered on a ligand in its bound state while appearing on the resonances of the free ligand. Transferred NOE experiments were carried out on samples containing 1 mM P18 peptide and 66 μM PduK. With approximately 15-fold excess of ligand and a moderate binding affinity, the peptide is in rapid exchange between free and bound states. NOEs indicative of the free state develop slowly. Thus, NOEs observed in the transferred NOE spectrum, at short mixing times, are indicative of the bound conformation of the peptide.

At short mixing times (100 ms) the observed NOE contacts were almost identical to the control NOESY spectra obtained in the absence of PduK, which indicates that there is no structural change upon binding. The major difference was an increased maximal NOE intensity and an increased rate of NOE build-up in the presence of the binding partner PduK (Figure 3). The increase in the rate of NOE build-up and intensity is due to the binding of the P18 peptide to the PduK protein, which enhances the cross relaxation rate due to the increase in the rotational correlation time. Our NMR data shows that the peptide is helical in solution, and the combination of STD and trNOE data support that this conformation is maintained while bound to the shell protein PduK.

In summary, the structure of the N-terminal region of PduP, P18, has been determined by NMR, revealing a strong helical structure. This structure is preformed and does not involve any significant conformational change with its binding partner (PduK), indicating a more general rather than a specific form of interaction. The fact that no significant structural change is required for binding suggests that the peptide adopts this conformation to reduce the entropic barrier for the interaction. Saturation transfer difference NMR has highlighted that one face of the helix shows the greatest interaction, involving several conserved hydrophobic residues. In particular the LIRNIL region contains the major molecular recognition features that allow for interaction with PduK. Our research has not identified the region of PduK to which the peptide binds. However, through analysis of C-terminal truncations we know that the binding region must lie in the N-terminal BMC domain between amino acids 1 and 96. Predictive modeling has suggested the C-terminal helix in PduA from *S. enterica* is responsible for the interaction with the internalized protein, PduP.[31] Similarly, the truncated PduK (PduK96) protein contains a homologous helix in this region that could be the potential site of interaction. This is suggestive of interactions between multiple shell proteins and P18 like targeting peptides. However, molecular detail on these interactions will require high-resolution structural data.

Fluorescein-Labeled P18 as a Reporter. To visualize the interaction between the BMC shell and the P18 peptide we have used fluorescence microscopy. The P18 peptide does not contain any lysine residues, and reaction with fluorescence isothiocyinate (FITC) produces a singularly labeled peptide at the N-terminal NH_3 group that is easily purified in high yield. Empty microcompartments, consisting of the shell proteins PduABJKNU, which were either unlabeled or contained PduA labeled with the fluorescent mCherry tag, were purified and incubated with the FITC-labeled P18 peptide. Following centrifugation to pellet the BMCs and remove any unbound P18, the BMCs were resuspended in buffer and visualized using a widefield microscope and optisplit (Cairn Research LTD) with appropriate filters (Supplementary Figure 8). Localization of green fluorescence was observed with the purified microcompartments. When the mCherry-labeled compartments were used, co-localization of the two fluorophores was observed, confirming that the FITC-P18 peptide is binding to the BMC shell. From these images it is not possible to determine if the peptide is binding to the outside or the inside of the BMCs. It is presumed that PduP must be located in the lumen and therefore is unlikely to interact with the outside of the shell; however, it could be possible that the peptide is able to access the interior of the microcompartment through one of the pores formed by the shell proteins. Such pores are large enough to allow access to cofactors such as cobalamin, coenzyme A, and NAD^+.

Localization of a Reporter Protein Using P18. To probe the internalization of proteins fused to the signaling sequence PduP18 into a BMC at higher resolution, we used a reporter protein that can be visualized by electron microscopy. Here, we fused the modified pea ascorbate peroxidase (APEX)[36] to the C-terminus of the P18 peptide. APEX allows for high resolution imaging of subcellular structures containing the enzyme by its ability to catalyze the H_2O_2-dependent polymerization of diaminobenzidine, generating an insoluble precipitate that stains with OsO_4. Thin sections of the strain producing the P18-APEX fusion protein and the shell proteins PduABJKNU were generated and viewed under TEM to reveal electron dense areas that match the shape and size of microcompartments (Figure 4), indicating that APEX is active when fused to P18 and that it is associated with the BMC where it catalyzes DAB polymer formation. No similar electron-dense areas were observed in sections of a control strain that contained the genes for the empty BMC and APEX without the P18 targeting peptide.

Through these experiments we have demonstrated that PduP is able to interact with the shell protein PduK and shown that P18 can bind to PduK with an affinity in the submicromolar range, consistent with tight binding. This level of binding explains how the proteins can interact but does not offer any insight into what happens to the targeted protein. Using isolated empty BMCs, which appear intact as viewed by TEM and AFM, addition of fluorescein-labeled P18 peptide results in localization of the peptide to the compartments *in vitro*. This likely reflects the strong interaction between P18 and the shell of the recombinant microcompartment. Further evidence that the P18 targeting sequence leads to co-localization of the protein to the microcompartment comes from *in vivo* analysis of cells producing P18-tagged APEX. Using this approach we have been able to show that dark regions of cells appear that are in agreement with the presence of BMCs and consistent with association of P18-tagged-APEX with the recombinant BMC. From our data it is not possible to determine whether APEX is internalized or just associated with the BMC. However, as previous work has shown that P18-GFP was encapsulated within the Pdu microcompartment, it is likely that other P18-tagged proteins are also internalized.[37]

Construction of an Ethanol Bioreactor. To generate the proof of principle that it is possible to incorporate pathways not natively associated with microcompartments into recombinant empty bacterial Pdu microcompartments, we chose to target

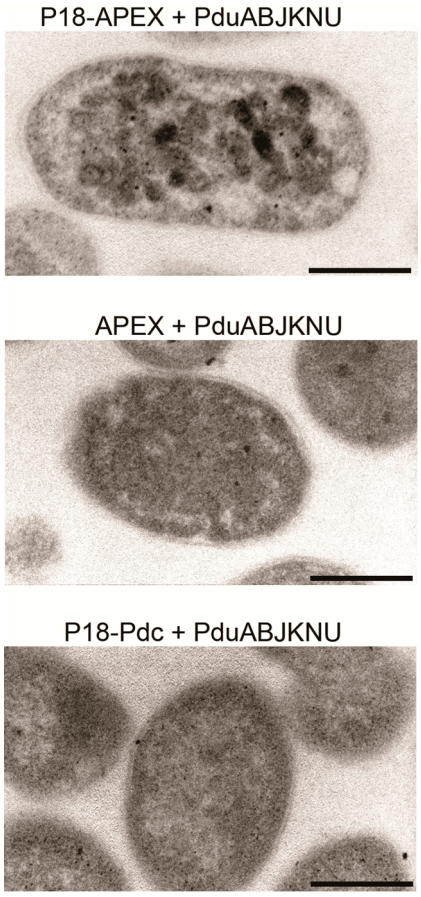

Figure 4. Localization of an EM reporter protein using P18. Transmission electron microscopy images of thin sections of *E. coli* BL21(DE3) carrying the genes for an empty microcompartment (*pduABJKNU*) and the EM reporter protein APEX fused to P18 (top), APEX (middle), or P18-Pdc (bottom). Before embedding, live cells were treated with DAB, the substrate for APEX, followed by staining with OsO_4. Sections of the P18-APEX strain show patches of electron density that match the size and shape of microcompartments, indicating that APEX is co-localized (right). These are not present in the APEX and P18-Pdc expressing strains. Scale bar is 0.5 μm.

the enzymes for the transformation of pyruvate to ethanol to an empty BMC. Ethanol production requires the heterologous expression of pyruvate decarboxylase (*pdc*) and alcohol dehydrogenase (*adh*) and their targeting to the protein shell (Figure 1). In this study the *pdc* and *adh* are derived from the strictly anaerobic ethanogenic Gram-negative bacterium *Z. mobilis*. The *pdc* gene was cloned so as to allow it to encode for an N-terminal fusion with the P18 targeting sequence. The *adh* gene was also initially cloned so as to encode a fusion with the first 18 amino acids of PduD (a D18 targeting sequence). Although the first 18 amino acids of PduD are sufficient for targeting proteins,[28] we also decided to explore an extended PduD sequence to allow for more space between PduD18 and the enzyme and thus chose to fuse the first 60 amino acids of PduD to Adh. The secondary structure prediction and SWISS-MODEL results of *C. freundii* PduD indicated that the first 18 residues are followed predominantly by a coiled secondary structure.

The tagged enzyme combinations, P18-Pdc D18-Adh and P18-Pdc D60-Adh, were investigated for their ability to target the enzymes efficiently to the BMC. Recombinant strains producing these enzymes were cultured for 96 h in LB medium supplemented with 4% glucose and compared to appropriate control strains. Growth rates and ethanol content (per OD_{600}) were recorded, which revealed that the co-expression of the shell proteins caused a growth delay up to 48 h compared to strains that produced only Pdc and Adh. However, around 48 h the strains producing shell proteins reached similar OD_{600} levels when compared to control strains (Supplementary Figure 9). At 48 h, in the absence of shell proteins, ethanogenic strains with a variety of tagged and untagged versions of Pdc and Adh produced similar amounts of alcohol (Pdc Adh: 36 ± 5 mM ethanol; P18-Pdc D18-Adh: 44 ± 11 mM ethanol; P18-Pdc D60-Adh: 38 ± 1 mM ethanol). However, in the presence of shell proteins the strains containing tagged Pdc and Adh produced more ethanol than the strain containing untagged Pdc and Adh (P18-Pdc D18-Adh: 59 ± 4 mM ethanol and P18-Pdc D60-Adh: 46 ± 1 mM ethanol versus Pdc Adh: 38 ± 8 mM) (Figure 5). The increase in ethanol production seen at 48

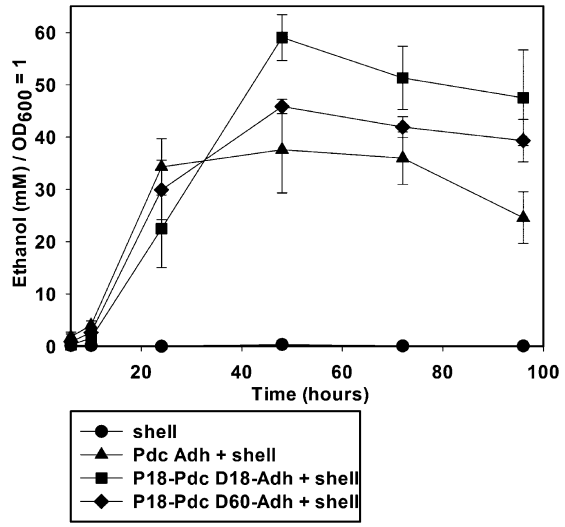

Figure 5. *In vivo* ethanol production. The graph shows the ethanol content (mM) of the growth medium of *E. coli* strains producing shell proteins only (●), shell proteins and untagged Pdc and Adh (▲), shell proteins and tagged Pdc and Adh (P18-Pdc D18-Adh is represented by ■, P18-Pdc and D60-Adh is represented by ◆). Ethanol concentration is normalized to OD_{600} = 1 and plotted from 6 to 96 h. Ethanol content was determined in triplicates and standard deviations are represented by error bars.

h in the P18-Pdc D18-Adh strain was shown to be statistically significant (p = 0.016) in comparison to the untagged control strain. By 96 h, the amount of ethanol measured in both the P18-Pdc D18-Adh (p = 0.015) and the P18-Pdc D60-Adh (p = 0.009) strains was higher than in the untagged control strain, differences that were verified by statistical analysis.

The elevation in ethanol production in strains containing targeted enzymes is coincident with the production of shell proteins. At 48 h, when the shell proteins were most abundant (Figure 6b and d), the strain producing shell proteins and P18-Pdc D18-Adh increased sharply in ethanol content (Figure 6a), producing more ethanol than the control strain without shell proteins. A similar, but less pronounced, effect was observed for the strain producing shell proteins and P18-Pdc D60-Adh (Figure 6c), but not for the untagged control strains (Supplementary Figure 10). SDS-PAGE analysis revealed that similar levels of P18-Pdc were present in strains that produced shell proteins when compared to strains that did not produce

dx.doi.org/10.1021/sb4001118 | *ACS Synth. Biol.* 2014, 3, 454−465

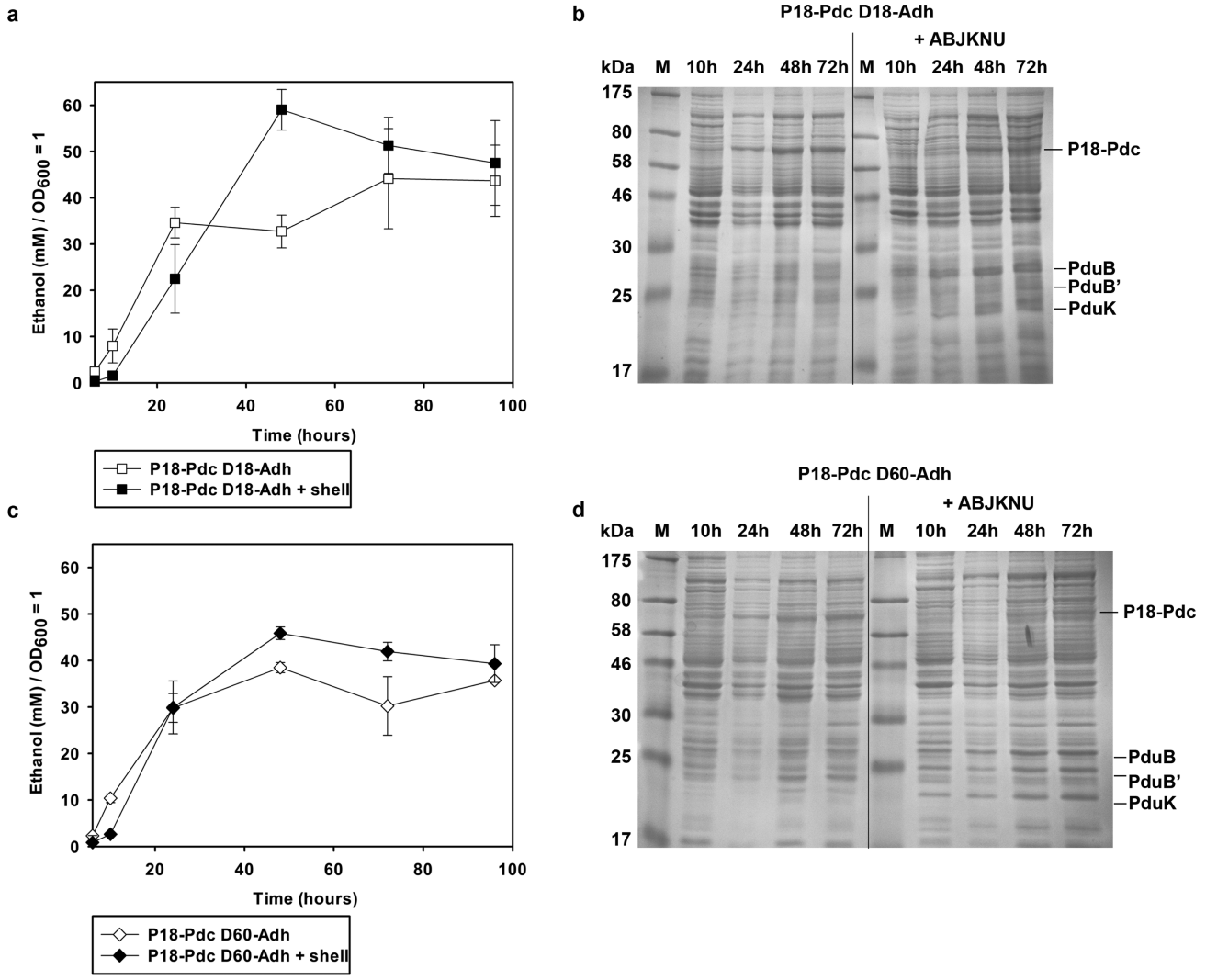

Figure 6. Ethanol production and protein profile in the presence and absence of shell proteins. The graphs show the ethanol content (mM) (normalized to OD_{600} = 1) over 96 h in the growth medium of *E. coli* strains producing (a) P18-Pdc D18-Adh (■, □) and (c) P18-Pdc D60-Adh (◆, ◇). Strains co-expressing the shell protein construct are indicated by solid symbols. Control strains without the shell protein construct are indicated by open symbols. The data are presented as an average of three independent experiments, and standard deviations are represented by error bars. Whole cell samples of (b) P18-Pdc D18-Adh and (d) P18-Pdc D60-Adh (± PduABJKNU) were adjusted to the same OD_{600} and analyzed by SDS-PAGE for their protein profiles.

shell proteins (Figure 6b, d). Thus, both Pdc and Adh are functional with and without their targeting sequences and apparently have similar levels of activity *in vivo*. However, targeting Pdc and Adh to the microcompartment improves ethanol production, suggesting either that the enzymes are more active when associated with the microcompartment or that the microcompartment enhances metabolic flux.

Purification of Recombinant Bioreactors. The activity of BMCs containing the Pdc and Adh were investigated by purifying the organelles. Bacteria containing the recombinant BMCs were lysed using Yeast Protein Extraction Reagent (YPER Plus), and the metabolosomes were separated from contaminating proteins on the basis of their differential solubility as described under microcompartment purification in the Methods section. The solubility of the BMC appears to be dependent on the NaCl concentration of the buffer (Figure 7). Low salt content (20 mM NaCl) increased their solubility, whereas higher salt content (80 mM NaCl) lowered their solubility. Analysis of the final protein fraction of purified empty microcompartments using TEM and AFM confirmed the presence of apparently intact irregularly shaped polygonal recombinant microcompartments around 100 nm in diameter (Figure 8a and b). Although not completely homogeneous, the purified microcompartment fraction was found to be enriched in shell proteins PduA, -B, -B′, -J, -K, -U when analyzed by SDS-PAGE (Figure 8c). PduN was not detectable in this profile, but as it is suspected to act as a vertex protein rather than making up the facets of the structure, it is likely to be present in only very small quantities.

When untagged Pdc and Adh are produced in the presence of an empty BMC, a small band at 64 kDa is present in the protein profile of microcompartments from this strain (Figure 8c). This band corresponds to the theoretical mass of Pdc (no band corresponding to the theoretical mass of Adh is visible). This suggests that some Pdc is either incorporated into the BMC in the absence of a signaling sequence or that some denatured Pdc co-purifies with the metabolosome.

dx.doi.org/10.1021/sb4001118 | *ACS Synth. Biol.* 2014, 3, 454−465

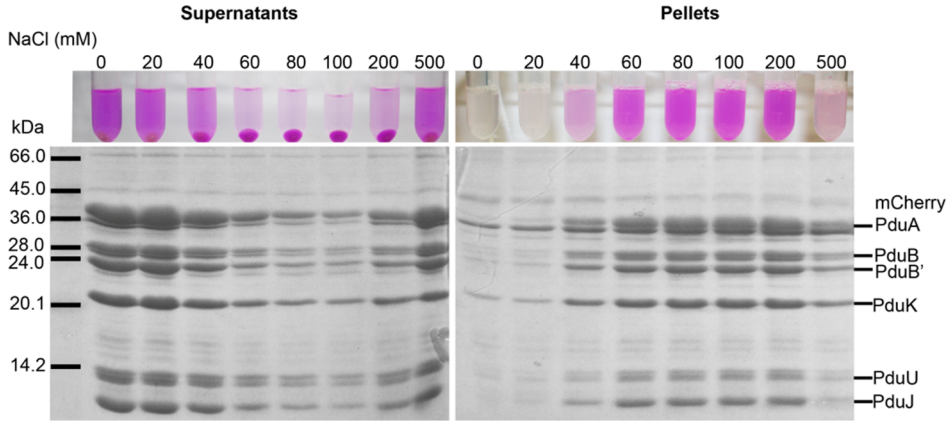

Figure 7. Solubility of microcompartments with respect to salt. To follow the microcompartments, colorometrically, PduA was tagged with mCherry, and compartments composed of mCherry-PduABB′JKNU were produced in BL21(DE3). The effect of NaCl concentration on the solubility of these colored isolated empty micrompartments was followed. After cell lysis in YPER Plus the lysate was centrifuged, and the resulting pellet was resuspended in 20 mM Tris-HCl (pH = 8.0) containing 0−500 mM NaCl. The suspension was centrifuged again, resulting in supernatant and pellet fractions, which were then analyzed by SDS-PAGE. The image on the left shows the tubes after centrifugation with the pellets still present and the image on the right shows the resuspended pellets after separation from the supernantants. Between 0 and 40 mM and at 500 mM NaCl the microcompartment proteins are soluble and are found in the supernatant fraction. Between 60 and 200 mM NaCl the microcompartments are less soluble and are found in the pellet fraction.

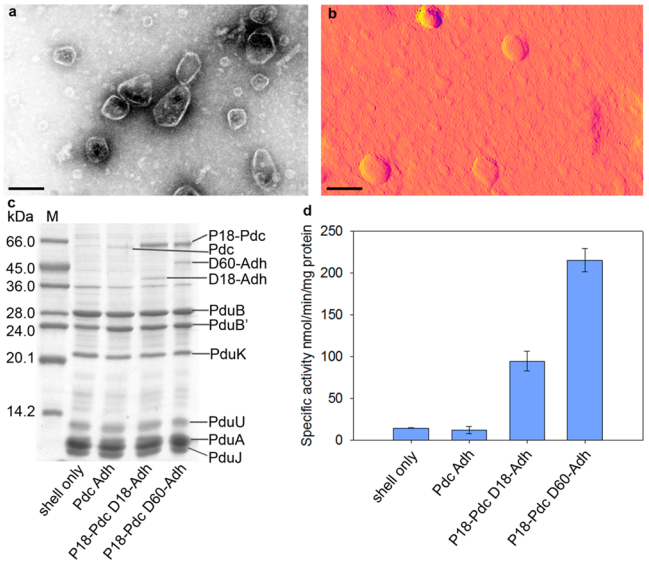

Figure 8. Isolation of recombinant bioreactors and determination of activity. (a) TEM and (b) AFM (peak force error) images of isolated empty microcompartments (PduABB′JKNU) showing how they purify as intact units (scale bar 100 nm). (c) SDS page loaded with 10 μg microcompartments purified from four strains co-producing PduA, -B, -B′, -J, -K, -N, -U and either no enzymes (shell only) or Pdc and Adh without signaling sequences (Pdc Adh) or P18-Pdc and D18-Adh or P18P-Pdc and D60-Adh. M is the SDS7 marker. (d) Specific activity of Adh in nmol NADH oxidized min^{-1} mg^{-1}. Activities were determined in triplicates with purified microcompartments isolated from the four strains described in panel c.

Purified microcompartments from strains producing Adh and Pdc with signaling sequences (P18-Pdc D18-Adh and P18-Pdc D60-Adh) co-purified with Pdc and Adh proteins (Figure 8c), indicating that both Pdc and Adh were interacting with the BMC through their signaling sequences. To determine if the purification protocol was specific for microcompartments, tagged and untagged Adh and Pdc were purified in the absence of the shell proteins PduA, -B, -B′, -J, -K, -U using the described purification method. No Adh or Pdc protein bands were detected in the final fraction of the purification (Supplementary Figure 11), suggesting that the Adh and Pdc can only be purified with microcompartments.

A Functional Ethanol Bioreactor. Purified microcompartments from the various strains were analyzed for their specific activity in the oxidation of NADH using a coupled assay that required both Pdc and Adh to be present and active (Figure 8d). The production of ethanol was confirmed separately by GC−MS. Microcompartments from the strain containing the P18-Pdc and D60-Adh had the highest NADH oxidation activity of 215 nmol NADH oxidized min^{-1} mg^{-1}, which was approximately 20 times higher than the specific activity of microcompartments extracted from cells producing untagged Adh and Pdc. Microcompartments purified from the strain producing the P18-Pdc and D60-Adh were twice as active as microcompartments from the strain producing P18-Pdc and D18-Adh. It is possible that the shorter PduD18 sequence might constrain Adh activity and thus lead to lower activity *in vitro*.

The foregoing experiments were undertaken to see if the P18 targeting sequence could be used to direct a small pathway to an empty BMC as a proof of concept that microcompartments can be engineered to perform new metabolic activities. We sought to target a pyruvate decarboxylase and alcohol dehydrogenase to the BMC since this would allow for ethanol production. We found that the P18 sequence allowed for the targeting of the *Z. mobilis* Pdc to the BMC, but strangely the P18 did not work well with the *Z. mobilis* Adh, as it was not possible to obtain a stable *E. coli* strain containing the shell protein construct and a P18-*pdc* P18-*adh* construct. We thus chose another targeting sequence, the N-terminal region of PduD, and constructed two different tags, one of 18 amino acids (D18) and a longer one of 60 amino acids (D60). Both of these sequences allowed for the targeting of Adh to the BMC. However, microcompartments isolated from the strain with the P18-*pdc* D60-*adh* were more active *in vitro*, although *in vivo* this strain produced less ethanol than the D18-Adh variant. It is not obvious what is the underlying cause to this anomaly, but it

dx.doi.org/10.1021/sb4001118 | *ACS Synth. Biol.* 2014, 3, 454−465

could be due to subtle differences in the level of Pdc and the net rate of flux under nonsaturating conditions.

Nonetheless, we have shown that it is possible to direct both P18-Pdc and D18-Adh or D60-Adh to the same BMC and produce a microcompartment that has the ability to convert pyruvate into ethanol. The compartment does increase the ethanogenic potential for *E. coli* as the amount of ethanol produced by cells containing tagged enzymes is higher than for cells expressing cytoplasmically located enzymes. It is also striking that ethanol production increases only with the appearance of larger quantities of shell proteins. Therefore, the bacterial microcompartments appear to afford protection to the cell in allowing the production of higher levels of ethanol, possibly through conservation of the volatile acetaldehyde intermediate.[38]

In conclusion, we have determined the structure of a BMC-targeting peptide (P18) and identified its major recognition epitopes. We have shown how this peptide from PduP and a related peptide from PduD are able to target enzymes to a recombinant BMC. We have used a high-resolution ascorbate peroxidase (APEX) system to demonstrate that the P18 peptide results in the association of the protein cargo within the BMC, and by using these targeting sequences we have generated a recombinant ethanol-producing bioreactor. This report therefore provides evidence that BMCs can be easily manipulated for the construction of new purposes and hold significant potential especially for processes that involve toxic intermediates. BMCs represent a subcellular compartment that is apposite for the redesign of biological processes.

METHODS

Bacterial Strains and Media. Strains and plasmids used in this study are listed in Supplementary Table 4. *E. coli* JM109 was used for routine cloning procedures. *E. coli* strain BL21(DE3) was used for the expression of the genes for ethanol production (*pdc* and *adhB from Z. mobilis*) and the genes encoding the shell proteins PduA, -B, -B′, -J, -K, -N, -U. Strains were grown in Luria−Bertani (LB) medium supplemented with antibiotics (50 μg/mL ampicillin, 35 μg/mL chloramphenicol, chloramphenicol stock dissolved in methanol at 10 mg/mL) as needed. All strains were grown at 37 °C and 160 rpm. Isolated colonies of *E. coli* strains were grown overnight in liquid medium and used as inoculum into fresh medium at a starting OD_{600} = 0.05, unless otherwise indicated. At OD_{600} = 0.8 protein production was induced with 400 μM IPTG overnight at 18 °C. Growth rates were recorded for 96 h in cultures (500 mL of LB) supplemented with 4% glucose at 28 °C, shaking at 160 rpm. Samples (1 mL) were taken for OD_{600} readings at 1, 2, 3, 4, 5, 6, 10, 24, 48, 72, and 96 h.

Pull-Down Assays. Pull-down assays were conducted between PduP and the seven individual shell proteins. Two constructs were co-expressed in *E. coli* BL21(DE3). The first plasmid (pET14b) contained one of the shell proteins as an N-terminal His-tag fusion. The second plasmid (pLysS) contained the gene encoding PduP without any tag. The transformants were grown in 1 L of Luria−Bertani medium to an OD_{600} of 0.8, when protein production was induced with 400 mM IPTG at 16 °C overnight. The cells were harvested by centrifugation at 4,000*g* at 4 °C for 10 min and resuspended in 10 mL of binding buffer (20 mM Tris-HCl pH 8.0, 0.5 M NaCl, 10 mM imidazole). The cells were lysed by sonication (six 30-s bursts, with 30-s cooling intervals on ice at an amplitude of 65%), and insoluble debris was removed by centrifugation at 37,000*g* for 15 min. The supernatant was applied to a chelating sepharose column charged with Ni^{2+}. Once bound to the column, the crude extract was subjected to washes containing stepwise increases in imidazole concentration up to 400 mM. All wash fractions were analyzed by SDS-PAGE to confirm coelution of the His-tagged and untagged proteins. The identities of the eluted proteins were confirmed by peptide mass fingerprinting. As a negative control, the His-tagged shell protein was omitted, and under these conditions no PduP was present in the elution fractions (as determined by SDS-PAGE).

NMR. Peptide structural NMR data sets were obtained at 283 K using a 14.1 T (600 MHz ^{1}H) Bruker Avance III NMR spectrometer equipped with a QCI-F cryoprobe. All NMR samples were 330 μL within a Shigemi NMR tube and contained 1 mM P18 peptide in 20 mM potassium phosphate buffer at pH 7.0 containing 100 mM sodium chloride and 9% (v/v) deuterium oxide. NMR data processing was completed using TopSpin 3.1 (Bruker), and assignments were completed using CCPN Analysis.[39] Data sets for structural determination were collected in the absence and presence of 30% (v/v) trifluoroethanol-d_3 (TFE). ^{1}H chemical shifts and through-space structural assignments were obtained from two-dimensional TOCSY[40] and NOESY[41] NMR experiments with mixing times of 80 and 350 ms, respectively (Supplementary Figure 3; Supplementary Table 1). Structural ensembles were calculated using CNS[42] and included dihedral angles confirmed using DANGLE.[43] The final ensemble of each structure was water-minimized using YASARA Structure software (available from http://www.yasara.org). Supplementary Table 2 refinement statistics together with Supplementary Figures 6 and 7 confirm the precision and quality of each peptide structure.

Standard ^{1}H STD NMR experiments with a 3-9-19 WATERGATE were performed using 1 mM P18 peptide with 15 μM PduK in the same PBS buffer system used for structure calculations in the absence of TFE. Gaussian STD excitation pulses of 20 ms duration and a γB_1 of 140 Hz were applied for 2 s at −3 ppm and −30 ppm for saturation and control, respectively, with on/off interleaved and extracted after the experiment (Supplementary Figure 5). The experiment, when repeated with saturation at +13 ppm and control at −30 ppm, produced the same overall result but at lower intensity due to reduced spin diffusion. ^{1}H T_1 relaxation time constants for the P18 peptide were obtained using an inversion−recovery sequence that included a 3-9-19 WATERGATE.[44] Inversion recovery 180°-τ-90° delays used to obtain T_1 were in 0.1 s steps between 0.2 and 1.0 s. ^{1}H T_1 values were then used to obtain quantitative STD NMR (qSTD) amplification factors using the GEM-CRL method described previously.[45] Intensities for STD and T_1 relaxation experiments obtained using Spectrus Processor (ACD Laboratories)

2D trNOE spectra were measured at mixing times of 50, 100, 150, 200, 250, 300, 350, and 400 ms using 1 mM P18 peptide and 66 μM PduK (15-fold ligand excess) in 20 mM potassium phosphate buffer at pH 7.0 containing 100 mM sodium chloride and 9% (v/v) deuterium oxide.

Localization of APEX Using P18. To probe internalization of a protein fused to PduP18 into recombinant microcompartments, the electron microscopy (EM) reporter protein APEX[36] was fused to the C-terminus of PduP18 (pET14b-*pduP18-APEX*). The control plasmid contained APEX alone (pET14b-*APEX*). APEX is a monomeric and activity enhanced mutant of pea ascorbate peroxidase and is expressed and reacted in live cells where it catalyzes the oxidative polymerization of

diaminobenzidine (DAB) to generate a cross-linked and locally deposited precipitate. EM contrast is created when the DAB polymer is stained with electron-dense OsO_4. The protocol was adapted from Martell *et al.*[36] as follows. The *E. coli* strain BL21(DE3) was co-transformed with pLysS-*pduABB′JKNU*, the plasmid encoding the shell proteins that form empty microcompartments and pET14b-*APEX* or pET14b-*pduP18-APEX*. Ten-milliliter LB starter cultures containing appropriate antibiotics and 1 colony were cultured for 6 h at 37 °C at 160 rpm and then inoculated into 50 mL of 2YT at starting OD_{600} = 0.01. The strains were incubated for 16 h at 37 °C at 160 rpm and then harvested by centrifugation. Next, 0.05 g of wet cells was washed 3 × 5 min in 1 mL of 100 mM sodium cacodylate, 2 mM $CaCl_2$, pH 7.4. The cells were resuspended in 1 mL of freshly made solution of 0.5 mg/mL (1.4 mM) DAB tetrahydrochloride, combined with 0.03% (v/v) H_2O_2 in chilled 100 mM sodium cacodylate, 2 mM $CaCl_2$, pH 7.4. After 1 min of incubation the cells were washed 3 × 5 min in 100 mM sodium cacodylate, 2 mM $CaCl_2$, pH 7.4 followed by 60 min of fixation at room temperature in 1 mL of 2% glutaraldehyde in 100 mM sodium cacodylate, 2 mM $CaCl_2$, pH 7.4. The cells were washed 3 × 5 min in 1 mL of chilled buffer, followed by post fixation staining with 2% osmium tetroxide for 60 min in chilled buffer. The cells were rinsed 3 × 5 min in chilled distilled water and placed in 30% ethanol overnight at 4 °C. The samples were dehydrated in a cold graded ethanol series, 10 min each (50%, 70%, 90%, 100%, 100%) and then washed once in room temperature anhydrous ethanol (to avoid condensation) followed by infiltration with LV resin (Agar Scientific): 1:1 (v/v) anhydrous ethanol and resin for 60 min. The cells were incubated twice in 100% LV resin for 1 h and finally transferred into fresh resin and polymerized at 60 °C for 16 h. Then, 85-nm sections were collected on 300 mesh copper grids and visualized under the TEM as described previously.[24]

Construction of Plasmids for Ethanol Production. *Pdc* was amplified by PCR using 5′-CATCATATGAGTTATACTGTCGG-3′ (forward primer) and 5′-CATGAATTCAAAACTAGTCAGAGGAGCTTGTTAACAGGC-3′ (reverse primer) introducing restriction sites *Nde*I (5′) and *Spe*I and *Eco*RI (3′) (all underlined). *Pdc* was cloned via *Nde*I and *Eco*RI sites into a modified pET23b-P18 (pSF59) allowing for the fusion of P18 and the 5′ end of *pdc*, creating pSN5. *Adh* was amplified by PCR using 5′-CACGAGCTCATGGCTTCTTCAACTTTTTATATTCC-3′ (forward primer) and 5′- CACGAATTCAAAACTAGTCAGAAAGCGCTCAGGAAGAGTTC-3′ (reverse primer) introducing restriction sites *Sac*I (5′) and *Spe*I and *Eco*RI (3′). *Adh* was cloned via *Sac*I and *Spe*I sites into pET3a containing *D18* and *D60* signaling sequences allowing for the fusion of the 3′ end of *D18* or *D60* and the 5′ end of *adh*, creating pSF61 and pSF63, respectively. Finally, two constructs were built housing *D18-adh* and *P18-pdc* (pSF64) and *D60-adh* and *P18-pdc* (pSF65). A plasmid with *adh* and *pdc* (pSN4) only was constructed as negative control.

Solubility Study of the Shell Proteins. BL21(DE3) was transformed with pLysS-*mCherry-pduA-BB′JKNU*, the plasmid encoding the shell proteins that form empty microcompartments[24] with PduA fused to a red fluorescent mCherry tag. The strain was cultured and the cells lysed as described in the next section. The cell lysate was aliquoted into eight 2-mL samples and centrifuged (5 min at 11,300*g*, 4 °C). The pellets were resuspended in 1 mL of 20 mM Tris-HCl, pH = 8.0 containing increasing concentrations of NaCl (0, 20, 40, 60, 80, 100, 200, 500 mM). The suspension was pelleted (5 min at 11,300*g*, 4 °C), and supernatants and pellets were collected and analyzed by SDS-PAGE. The mCherry tag allowed the visualization of the shell proteins.

Microcompartment Purification. BL21(DE3) strains containing genes for BMC formation were cultured in 200 mL of LB medium, and the cells were harvested by centrifugation for 10 min at 4 °C at 2683*g*. One gram of wet cell pellet was resuspended in 10 mL of YPER Plus (Pierce) supplemented with 1 tablet of Complete Protease Inhibitor Cocktail (Roche) and 1250 units Benzonase Nuclease (YPB) and incubated for 3 h at room temperature under gentle agitation.

As outlined above we observed that the shell proteins varied in solubility depending on the salt concentration of the buffer they were resuspended in. This property was used to separate the shell proteins from other proteins by subjecting the samples to varying salt concentrations as follows: The lysate was pelleted for 5 min at 11,300*g* (Beckman Coulter, rotor JA 25.50), and the microcompartment-containing pellet was collected. The pellet was resuspended in 2 mL of 20 mM Tris-HCl, pH 8.0, 20 mM NaCl. The suspension was centrifuged at 4 °C for 5 min at 11,000*g* (Multispeed Refrigerated Centrifuge, ALC PK121R), and the supernatant, which contained the solubilized microcompartments, was collected. The NaCl concentration of the supernatant was raised to 80 mM by addition of 5 M NaCl. The microcompartments became insoluble, and the cloudy solution was centrifuged at 4 °C for 5 min at 11,000*g*. The pellet with the microcompartments was collected, resuspended in 1 mL of 20 mM Tris-HCl, pH 8.0, and finally clarified by centrifugation (5 min at 11,000*g*). The final supernatant was collected for further analysis.

EM and AFM. For EM analysis 10 μL of purified microcompartments were mounted onto Formvar, carbon coated 600 mesh copper grids for 2 min, followed by the addition of 20 μL of 2.5% (v/v) glutaraldehyde in PBS for 1 min. The grids were washed three times in 20-μL drops of 2.5% (v/v) glutaraldehyde in PBS and then three times in water. Finally the grids were dried and stained with 2% aqueous uranyl acetate.

AFM images were collected on a Bruker Multimode 8 scanning probe microscope. Purified BMCs were deposited on a graphite substrate by incubating 20 μL of sample on a freshly cleaved HOPG surface for 5 min. The sample was then fixed using 2.5% (v/v) glutaraldehyde in PBS and dried with a gentle stream of N_2 gas. Images were collected in air using the peak-force tapping mode with peak-asyst air cantilever probe (Bruker) with a nominal spring constant of 0.4 N/m and processed using the supplied Nanoscope software.

Activity Assays. The activities of Pdc and Adh were monitored spectrophotometrically by measuring the absorbance change at 340 nm due to the oxidation of NADH. The assay depended on the conversion of pyruvate to acetaldehyde, catalyzed by Pdc and required Adh as the coupling enzyme to facilitate NADH oxidation. The reaction was carried out at room temperature in 20 mM Tris-HCl, pH 8.0. One-milliliter reactions contained 5 mM pyruvate, 0.15 mM NADH, 5 mM $MgCl_2$, 0.1 mM thiamine pyrophosphate and 481 μg of purified microcompartments. The reaction was started by addition of pyruvate and NADH, and the rate of NADH oxidation was measured at 340 nm.

Analysis of Ethanol Production. *In vivo* ethanol production was determined by analysis of the growth medium

dx.doi.org/10.1021/sb4001118 | *ACS Synth. Biol.* 2014, 3, 454−465

after culturing the strains. Cultures (500 mL of LB) supplemented with 4% glucose were grown for 96 h at 28 °C, shaking at 160 rpm. Samples (2 mL) were taken for GC analysis at 6, 10, 24, 48, 72, and 96 h. Cells were removed by centrifugation, and the growth medium was subjected to GC−MS analysis. Statistical analysis of the ethanol produced by each of the strains was performed in Minitab Statistical Software version 16.1 using either a one-way ANOVA (Analysis of Variance) at the 95% level with posthoc analysis by Turkey's test or *t* test.

Purified microcompartments were tested for their ability to convert pyruvate to ethanol by overnight incubation at room temperature in 1-mL reactions containing 50 mM pyruvate, 50 mM NADH, 50 mM $MgCl_2$, 1 mM thiamine pyrophosphate, and 1.6 mg of protein. The reactions were clarified by centrifugation for 10 min, and the supernatant was filtered through a vivaspin column (molecular cut off 10,000 Da). The filtrate was analyzed for ethanol content by GC−MS.

As commercial NADH (Sigma) contains traces of ethanol, NADH used in the reaction was produced using alternative published methods[46−48] by incubation of 0.03 M glucose, 0.015 M NAD^+, and 35 U of Glucose dehydrogenase in 0.05 M sodium bicarbonate, pH 7.5 at 37 °C overnight. NADH was purified on DEAE in a 0−0.2 M ammonium bicarbonate gradient. After two cycles of rotary evaporation NADH was resuspended in Millipore water.

■ ASSOCIATED CONTENT

Supporting Information

This material is available free of charge via the Internet at http://pubs.acs.org.

■ AUTHOR INFORMATION

Corresponding Author

*Tel: 00 44 (0)1227 824690. E-mail: m.j.warren@kent.ac.uk.

Author Contributions

#These authors contributed equally to this work.

Notes

The authors declare no competing financial interest.

■ ACKNOWLEDGMENTS

This work was supported by grants from the Biotechnology and Biological Sciences Research Council (BBSRC) BB/H013180/1 and BB/E024203/1 and The Welcome Trust 091163/Z/10/Z. We thank Kevin Howland for synthesis of the P18 peptide and technical support for GC−MS, Luke Lloyd for cloning of the APEX gene, and Emma Hargreaves for help with the statistical analysis.

■ REFERENCES

(1) Frank, S., Lawrence, A. D., Prentice, M. B., and Warren, M. J. (2013) Bacterial microcompartments moving into a synthetic biological world. *J. Biotechnol. 163*, 273−279.

(2) Cannon, G. C., Bradburne, C. E., Aldrich, H. C., Baker, S. H., Heinhorst, S., and Shively, J. M. (2001) Microcompartments in prokaryotes: carboxysomes and related polyhedra. *Appl. Environ. Microbiol. 67*, 5351−5361.

(3) Iancu, C. V., Ding, H. J., Morris, D. M., Dias, D. P., Gonzales, A. D., Martino, A., and Jensen, G. J. (2007) The structure of isolated Synechococcus strain WH8102 carboxysomes as revealed by electron cryotomography. *J. Mol. Biol. 372*, 764−773.

(4) Iancu, C. V., Morris, D. M., Dou, Z., Heinhorst, S., Cannon, G. C., and Jensen, G. J. (2010) Organization, structure, and assembly of alpha-carboxysomes determined by electron cryotomography of intact cells. *J. Mol. Biol. 396*, 105−117.

(5) Kerfeld, C. A., Heinhorst, S., and Cannon, G. C. (2010) Bacterial microcompartments. *Annu. Rev. Microbiol. 64*, 391−408.

(6) Schmid, M. F., Paredes, A. M., Khant, H. A., Soyer, F., Aldrich, H. C., Chiu, W., and Shively, J. M. (2006) Structure of Halothiobacillus neapolitanus carboxysomes by cryo-electron tomography. *J. Mol. Biol. 364*, 526−535.

(7) Tanaka, S., Kerfeld, C. A., Sawaya, M. R., Cai, F., Heinhorst, S., Cannon, G. C., and Yeates, T. O. (2008) Atomic-level models of the bacterial carboxysome shell. *Science 319*, 1083−1086.

(8) Havemann, G. D., and Bobik, T. A. (2003) Protein content of polyhedral organelles involved in coenzyme B12-dependent degradation of 1,2-propanediol in Salmonella enterica serovar Typhimurium LT2. *J. Bacteriol. 185*, 5086−5095.

(9) Havemann, G. D., Sampson, E. M., and Bobik, T. A. (2002) PduA is a shell protein of polyhedral organelles involved in coenzyme B-12-dependent degradation of 1,2-propanediol in Salmonella enterica serovar typhimurium LT2. *J. Bacteriol. 184*, 1253−1261.

(10) Kofoid, E., Rappleye, C., Stojiljkovic, I., and Roth, J. (1999) The 17-gene ethanolamine (eut) operon of Salmonella typhimurium encodes five homologues of carboxysome shell proteins. *J. Bacteriol. 181*, 5317−5329.

(11) Parsons, J. B., Dinesh, S. D., Deery, E., Leech, H. K., Brindley, A. A., Heldt, D., Frank, S., Smales, C. M., Lunsdorf, H., Rambach, A., Gass, M. H., Bleloch, A., McClean, K. J., Munro, A. W., Rigby, S. E., Warren, M. J., and Prentice, M. B. (2008) Biochemical and structural insights into bacterial organelle form and biogenesis. *J. Biol. Chem. 283*, 14366−14375.

(12) Stojiljkovic, I., Baumler, A. J., and Heffron, F. (1995) Ethanolamine utilization in Salmonella typhimurium: nucleotide sequence, protein expression, and mutational analysis of the cchA cchB eutE eutJ eutG eutH gene cluster. *J. Bacteriol. 177*, 1357−1366.

(13) Brinsmade, S. R., Paldon, T., and Escalante-Semerena, J. C. (2005) Minimal functions and physiological conditions required for growth of salmonella enterica on ethanolamine in the absence of the metabolosome. *J. Bacteriol. 187*, 8039−8046.

(14) Bobik, T. A., Havemann, G. D., Busch, R. J., Williams, D. S., and Aldrich, H. C. (1999) The propanediol utilization (pdu) operon of Salmonella enterica serovar Typhimurium LT2 includes genes necessary for formation of polyhedral organelles involved in coenzyme B(12)-dependent 1, 2-propanediol degradation. *J. Bacteriol. 181*, 5967−5975.

(15) Sriramulu, D. D., Liang, M., Hernandez-Romero, D., Raux-Deery, E., Lunsdorf, H., Parsons, J. B., Warren, M. J., and Prentice, M. B. (2008) Lactobacillus reuteri DSM 20016 produces cobalamin-dependent diol dehydratase in metabolosomes and metabolizes 1,2-propanediol by disproportionation. *J. Bacteriol. 190*, 4559−4567.

(16) Crowley, C. S., Cascio, D., Sawaya, M. R., Kopstein, J. S., Bobik, T. A., and Yeates, T. O. (2010) Structural insight into the mechanisms of transport across the Salmonella enterica Pdu microcompartment shell. *J. Biol. Chem. 285*, 37838−37846.

(17) Yeates, T. O., Crowley, C. S., and Tanaka, S. (2010) Bacterial microcompartment organelles: protein shell structure and evolution. *Annu. Rev. Biophys. 39*, 185−205.

(18) Yeates, T. O., Kerfeld, C. A., Heinhorst, S., Cannon, G. C., and Shively, J. M. (2008) Protein-based organelles in bacteria: carboxysomes and related microcompartments. *Nat. Rev. Microbiol. 6*, 681−691.

(19) Yeates, T. O., Thompson, M. C., and Bobik, T. A. (2011) The protein shells of bacterial microcompartment organelles. *Curr. Opin. Struct. Biol. 21*, 223−231.

(20) Wheatley, N. M., Gidaniyan, S. D., Liu, Y., Cascio, D., and Yeates, T. O. (2013) Bacterial microcompartment shells of diverse functional types possess pentameric vertex proteins. *Protein Sci. 22*, 660−665.

(21) Kerfeld, C. A., Sawaya, M. R., Tanaka, S., Nguyen, C. V., Phillips, M., Beeby, M., and Yeates, T. O. (2005) Protein structures forming the shell of primitive bacterial organelles. *Science 309*, 936−938.

(22) Tanaka, S., Sawaya, M. R., and Yeates, T. O. (2010) Structure and mechanisms of a protein-based organelle in Escherichia coli. *Science 327*, 81−84.
(23) Pang, A., Liang, M., Prentice, M. B., and Pickersgill, R. W. (2012) Substrate channels revealed in the trimeric Lactobacillus reuteri bacterial microcompartment shell protein PduB. *Acta Crystallogr., Sect. D: Biol. Crystallogr. 68*, 1642−1652.
(24) Parsons, J. B., Frank, S., Bhella, D., Liang, M., Prentice, M. B., Mulvihill, D. P., and Warren, M. J. (2010) Synthesis of empty bacterial microcompartments, directed organelle protein incorporation, and evidence of filament-associated organelle movement. *Mol. Cell 38*, 305−315.
(25) Bonacci, W., Teng, P. K., Afonso, B., Niederholtmeyer, H., Grob, P., Silver, P. A., and Savage, D. F. (2012) Modularity of a carbon-fixing protein organelle. *Proc. Natl. Acad. Sci. U.S.A. 109*, 478−483.
(26) Chen, A. H., Robinson-Mosher, A., Savage, D. F., Silver, P. A., and Polka, J. K. (2013) The bacterial carbon-fixing organelle is formed by shell envelopment of preassembled cargo. *PLoS One 8*, e76127.
(27) Cameron, J. C., Wilson, S. C., Bernstein, S. L., and Kerfeld, C. A. (2013) Biogenesis of a bacterial organelle: the carboxysome assembly pathway. *Cell 155*, 1131−1140.
(28) Fan, C., and Bobik, T. A. (2011) The N-terminal region of the medium subunit (PduD) packages adenosylcobalamin-dependent diol dehydratase (PduCDE) into the Pdu microcompartment. *J. Bacteriol. 193*, 5623−5628.
(29) Fan, C. G., Cheng, S., Liu, Y., Escobar, C. M., Crowley, C. S., Jefferson, R. E., Yeates, T. O., and Bobik, T. A. (2010) Short N-terminal sequences package proteins into bacterial microcompartments. *Proc. Natl. Acad. Sci. U.S.A. 107*, 7509−7514.
(30) Kinney, J. N., Salmeen, A., Cai, F., and Kerfeld, C. A. (2012) Elucidating essential role of conserved carboxysomal protein CcmN reveals common feature of bacterial microcompartment assembly. *J. Biol. Chem. 287*, 17729−17736.
(31) Fan, C., Cheng, S., Sinha, S., and Bobik, T. A. (2012) Interactions between the termini of lumen enzymes and shell proteins mediate enzyme encapsulation into bacterial microcompartments. *Proc. Natl. Acad. Sci. U.S.A. 109*, 14995−15000.
(32) Meyer, B., and Peters, T. (2003) NMR Spectroscopy techniques for screening and identifying ligand binding to protein receptors. *Angew. Chem., Int. Ed. 42*, 864−890.
(33) Man, Y. K., Dicara, D., Chan, N., Vessillier, S., Mather, S. J., Rowe, M. L., Howard, M. J., Marshall, J. F., and Nissim, A. (2013) Structural guided scaffold phage display libraries as a source of biotherapeutics. *PloS One 8*, e70452.
(34) Wagstaff, J. L., Rowe, M. L., Hsieh, S.-J., DiCara, D., Marshall, J. F., Williamson, R. A., and Howard, M. J. (2012) NMR relaxation and structural elucidation of peptides in the presence and absence of trifluoroethanol illuminates the critical molecular nature of integrin [small alpha]v[small beta]6 ligand specificity. *RSC Adv 2*, 11019−11028.
(35) Povey, J. F., Smales, C. M., Hassard, S. J., and Howard, M. J. (2007) Comparison of the effects of 2,2,2-trifluoroethanol on peptide and protein structure and function. *J. Struct. Biol. 157*, 329−338.
(36) Martell, J. D., Deerinck, T. J., Sancak, Y., Poulos, T. L., Mootha, V. K., Sosinsky, G. E., Ellisman, M. H., and Ting, A. Y. (2012) Engineered ascorbate peroxidase as a genetically encoded reporter for electron microscopy. *Nat. Biotechnol. 30*, 1143−1148.
(37) Fan, C., Cheng, S., Liu, Y., Escobar, C. M., Crowley, C. S., Jefferson, R. E., Yeates, T. O., and Bobik, T. A. (2010) Short N-terminal sequences package proteins into bacterial microcompartments. *Proc. Natl. Acad. Sci. U.S.A. 107*, 7509−7514.
(38) Penrod, J. T., and Roth, J. R. (2006) Conserving a volatile metabolite: a role for carboxysome-like organelles in Salmonella enterica. *J. Bacteriol. 188*, 2865−2874.
(39) Vranken, W. F., Boucher, W., Stevens, T. J., Fogh, R. H., Pajon, A., Llinas, M., Ulrich, E. L., Markley, J. L., Ionides, J., and Laue, E. D. (2005) The CCPN data model for NMR spectroscopy: development of a software pipeline. *Proteins 59*, 687−696.
(40) Bruschweiler, R., and Ernst, R. R. (1992) Molecular-dynamics monitored by cross-correlated cross relaxation of spins quantized along orthogonal axes. *J. Chem. Phys. 96*, 1758−1766.
(41) Jeener, J., Meier, B. H., Bachmann, P., and Ernst, R. R. (1979) Investigation of exchange processes by 2-dimensional NMR-spectroscopy. *J. Chem. Phys. 71*, 4546−4553.
(42) Brunger, A. T., Adams, P. D., Clore, G. M., DeLano, W. L., Gros, P., Grosse-Kunstleve, R. W., Jiang, J. S., Kuszewski, J., Nilges, M., Pannu, N. S., Read, R. J., Rice, L. M., Simonson, T., and Warren, G. L. (1998) Crystallography & NMR system: A new software suite for macromolecular structure determination. *Acta Crystallogr., Sect. D: Biol. Crystallogr. 54* (Pt 5), 905−921.
(43) Cheung, M. S., Maguire, M. L., Stevens, T. J., and Broadhurst, R. W. (2010) DANGLE: A Bayesian inferential method for predicting protein backbone dihedral angles and secondary structure. *J. Magn. Reson. 202*, 223−233.
(44) Piotto, M., Saudek, V., and Sklenar, V. (1992) Gradient-tailored excitation for single-quantum NMR-spectroscopy of aqueous-solutions. *J. Biomol. NMR 2*, 661−665.
(45) Kemper, S., Patel, M. K., Errey, J. C., Davis, B. G., Jones, J. A., and Claridge, T. D. (2010) Group epitope mapping considering relaxation of the ligand (GEM-CRL): including longitudinal relaxation rates in the analysis of saturation transfer difference (STD) experiments. *J. Magn. Reson. 203*, 1−10.
(46) Gassner, G., Wang, L., Batie, C., and Ballou, D. P. (1994) Reaction of phthalate dioxygenase reductase with NADH and NAD: kinetic and spectral characterization of intermediates. *Biochemistry 33*, 12184−12193.
(47) Hauck, T., Landmann, C., Raab, T., Bruhlmann, F., and Schwab, W. (2002) Chemical formation of 4-hydroxy-2,5-dimethyl-3[2H]-furanone from D-fructose 1,6-diphosphate. *Carbohydr. Res. 337*, 1185−1191.
(48) Margolis, S., Howell, B. F., and Schaffer, R. (1976) Purification and analysis of the purity of NADH. *Clin. Chem. 22*, 1322−1329.